Journal of Asian Ceramic Societies 4 (2016) 344–350

HOSTED BY

Contents lists available at ScienceDirect

Journal of Asian Ceramic Societies

journal homepage: www.elsevier.com/locate/jascer

Porosity and cell size control in alumina foam preparation by thermo-foaming of powder dispersions in molten sucrose

Sujith Vijayan, Praveen Wilson, K. Prabhakaran*

Department of Chemistry, Indian Institute of Space Science and Technology, Thiruvananthapuram 695 547, India

ARTICLE INFO

Article history:
Received 6 April 2016
Received in revised form 22 June 2016
Accepted 25 June 2016
Available online 14 July 2016

Keywords:
Foaming temperature
Alumina
Porosity
Foams
Sucrose
Strength

ABSTRACT

The foaming characteristics of alumina powder dispersions in molten sucrose have been studied as a function of alumina powder to sucrose weight ratio ($W_{A/S}$) and foaming temperature. The increase in foaming temperature significantly decreases the foaming and foam setting time and increases the foam volume due to an increase in the rate of —OH condensation as well as a decrease in the viscosity of the dispersion. Nevertheless, the foam collapses beyond a critical foaming temperature, which depends on the $W_{A/S}$. The sintering shrinkage depends mainly on the $W_{A/S}$ and marginally on the foaming temperature. The porosity (83.4–94.6 vol.%) and cell size (0.55–1.6 mm) increase with an increase in foaming temperature (120–170 °C) and a decrease in $W_{A/S}$ (0.8–1.6). The drastic decrease in compressive strength and modulus beyond a $W_{A/S}$ of 1.2 is due to the pores generated on the cell walls and struts as a result of particle agglomeration. Gibson and Ashby plots show large deviation with respect to the model constants '*C*' and '*n*', especially at higher alumina powder to sucrose weight ratios.

1. Introduction

Ceramic foams are low density materials with high specific strength, high surface area, low thermal conductivity and controlled permeability [1]. Due to this, they are used in a variety of applications such as high temperature thermal insulation, molten metal filtration, catalyst support, lightweight structural components and as a pre-form for polymer–ceramic and metal–ceramic composites [2–6]. Ceramic foams are generally prepared by the replication of polymer foams, foaming and setting of ceramic powder suspensions, and emulsion templating. In the first method, ceramic replica of a polymer foam template is produced by coating the polymer foam with a ceramic powder suspension followed by drying, burnout of the polymer foam template and sintering [7–9]. In the second method, foamed powder suspensions produced by stabilizing gas bubbles using either surfactant or particles with suitable wetting characteristic are cast in a mould [10–19]. The cast-foamed suspensions are then set by either in situ polymerization of organic monomers or by coagulation of the powder suspensions. The wet foam bodies are subsequently dried, binder removed and sintered to produce the ceramic foams. In the third method, immiscible liquid (oil) droplets are dispersed in a ceramic precursor sol or ceramic powder suspension using a suitable emulsifying agent to form an emulsion [20–27]. The emulsion is then set by gelation of the sol or ceramic powder suspension. The gelled emulsion body is dried, oil removed and sintered to produce the macroporous ceramic foams. Use of liquid droplet as pore template is advantageous, as a uniform dispersion of the immiscible liquid droplets in an aqueous slurry medium using an emulsifying agent could be obtained by simple stirring. Also, the pore size could be manipulated by controlling the droplet size, which can be obtained by adjusting the emulsifying agent concentration and mixing speed. High internal phase emulsions [24,27,28] with liquid template phase more than 74 vol.% are possible which leads to macroporous ceramics with very high porosity and highly interconnected pore structure.

Recently, we have reported a thermo-foaming of powder dispersions in molten sucrose for the preparation of alumina foams [29]. In this, alumina powder dispersions in molten sucrose were thermo-foamed at 150 °C to produce a sucrose polymer–alumina powder composite foam bodies. Subsequent sucrose polymer burnout and sintering produces well interconnected cellular ceramics with high porosity and relatively high compressive strength. The method is simple and does not use any toxic chemicals

* Corresponding author. Tel.: +91 471 2568535; fax: +91 471 2568541.
E-mail address: kp2952002@gmail.com (K. Prabhakaran).
Peer review under responsibility of The Ceramic Society of Japan and the Korean Ceramic Society.

http://dx.doi.org/10.1016/j.jascer.2016.06.007

as processing additives. Moreover, large sintered alumina ceramic bodies without any crack could be fabricated by this process by introducing an intermediate pyrolysis of the sucrose polymer before burnout and sintering [30]. Moreover, we have observed a slight increase in sintering shrinkage, decrease in porosity and increase in compressive strength by the intermediate pyrolysis of the sucrose polymer. However, the alumina foams produced by thermo-foaming at 150 °C from dispersions of alumina powder to sucrose weight ratios ($W_{A/S}$) in the range of 0.6–1.4 showed porosities in a close range of 93.3–94% [29]. The present work is an effort to control the porosity and cell size of the alumina foams to a wide range by controlling the foaming temperature as well as the $W_{A/S}$. The study also provides the effect of temperature and $W_{A/S}$ on the foaming time and foam setting time of alumina powder dispersions in molten sucrose. In the present work, the $W_{A/S}$ of 0.8 and above is used, as cracks were often formed during sintering of the foam bodies prepared at a $W_{A/S}$ below 0.8 [30].

2. Experimental

α-Alumina powder (A16SG, ACC Alcoa, Kolkata) of 0.34 μm average particle size and specific surface area of 10.4 m^2/g was used. Analytical reagent grade sucrose and acetone used were procured from Merck India Ltd., Mumbai. The procedure for thermo-foaming of alumina powder dispersions in molten sucrose reported in our previous publication was adopted without any modification [29]. The sucrose (200 g) and alumina powder in various weight ratios were intimately mixed by planetary ball milling (Fritsch, Germany) at 200 rpm in acetone medium for 4 h using zirconia grinding media of 10 mm diameter in 500 ml zirconia jars. The slurries thus obtained were dried in glass trays at 80 °C in an air oven. The alumina powder–sucrose mixtures obtained after drying had $W_{A/S}$ in the range of 0.8–1. This corresponds to volume percentage of alumina in the mixtures in the range of 24.3–41.8 (density of sucrose – 1.59 g/cm^3). The sucrose–alumina powder mixtures were heated in 2.5 l borosilicate glass trays at 185 °C in an air oven to melt the sucrose. The melt was stirred well with a glass rod to get uniform dispersion of the alumina powder in the molten sucrose. The alumina powder dispersions in the molten sucrose were kept in an air oven at temperatures ranging from 120 to 180 °C for foaming and setting. The foams were cut into rectangular bodies of 10 cm × 10 cm × 4 cm and heated in an inert (Argon) atmosphere furnace at 900 °C for 2 h for pyrolysis of the sucrose polymer [30]. The heating rate used was 0.5 °C/min. The pyrolyzed foam bodies were heated in an electrically heated sintering furnace in air atmosphere up to 1600 °C for removal of the carbon and subsequent sintering. The heating rates used were 0.5 °C/min and 1 °C/min from room temperature to 600 °C and from 600 °C to 1600 °C, respectively. A holding time of 2 h was given at 600 °C and 1600 °C. The volume shrinkage of the bodies was calculated from the initial and final dimensions. The density of the alumina foam bodies was calculated from their weights and dimensions.

The viscosity measurement of the alumina powder dispersions in molten sucrose was carried out at various shear rates at temperatures ranging from 120 to 160 °C using a rheometer (MCR 102 Modular Compact Rheometer, Anton Paar, USA) with a cone and plate measurement system (CP-25, 25 mm diameter and angle 2°). The microstructure of the foams was observed using a scanning electron microscope (SEM, FEI Quanta FEG200). The cell size was measured on the magnified image of the alumina foams observed using a vision inspection system with a CCD colour camera (Vision 300 GL, TESA Technologies, Switzerland). The values reported were average of 25 measurements. The compressive strength of the alumina foams was measured according to the ASTM standard C365/C365-05 using rectangular samples of 25 mm × 25 mm × 12 mm size in a Universal Testing Machine (Instron 5500, Instron USA) at a loading rate of 0.5 mm/min.

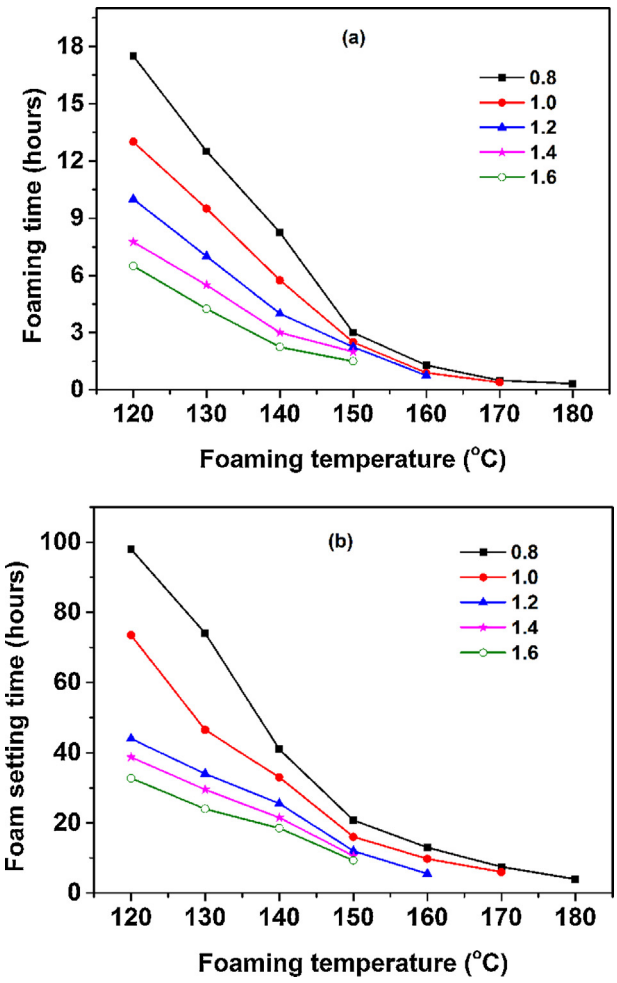

Fig. 1. Effect of foaming temperature on (a) foaming time and (b) foam setting time of dispersion at various $W_{A/S}$.

3. Results and discussion

It has been reported that the foaming and setting of alumina powder dispersions in molten sucrose is due to the —OH to —OH condensation between the glucose and fructose anhydride molecules formed from the sucrose [29]. That is, water vapour generated due to the condensation reaction is responsible for the foaming of the alumina powder dispersions. The bubble stabilization and setting of the foamed dispersions is due to viscosity increase by the continued condensation polymerization. The alumina particles in the dispersion promote foaming and foam setting by facilitating the —OH condensation. Further, the alumina particles adsorbed on the liquid–air interface offer additional bubble stability by the particle stabilization mechanism. Fig. 1 shows the effect of temperature on foaming and setting of alumina powder dispersions of various $W_{A/S}$. At all the studied $W_{A/S}$, the foaming time and foam setting time decrease significantly with an increase in foaming temperature. For example, the foaming time at a $W_{A/S}$ 0.8 decreases from 17.5 to 0.5 h when the foaming temperature increases from 120 to 170 °C. The corresponding decrease in foam setting time is from 98 to 7.5 h. On the other hand, at a particular foaming temperature, the foaming time and foam setting time increase with a decrease of $W_{A/S}$. The difference observed in foaming time and foam setting time between powder dispersions of

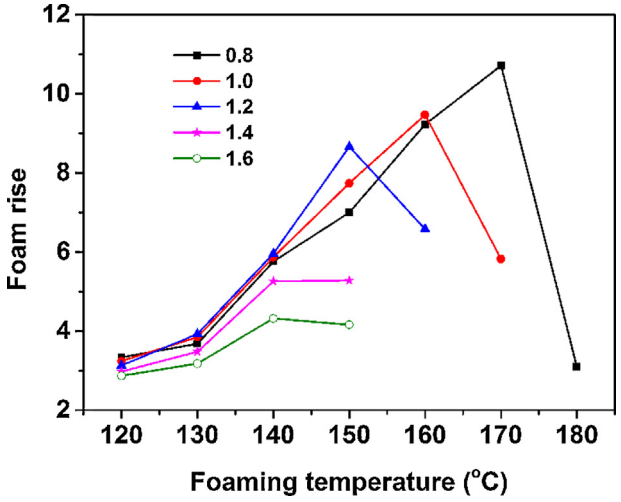

Fig. 2. Effect of foaming temperature and $W_{A/S}$ on the foam rise (ratio of the final foam height to the initial dispersion height) of alumina powder dispersions in molten sucrose.

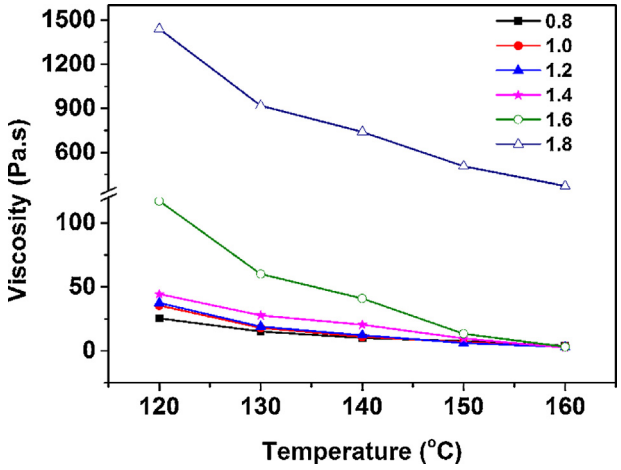

Fig. 3. Effect of temperature on the viscosity of the powder dispersion in molten sucrose at various $W_{A/S}$ (shear rate 10 s^{-1}).

consecutive $W_{A/S}$ is higher at lower foaming temperature. That is, at 120 °C, the foaming time decreases from 17.5 to 6.5 h when the $W_{A/S}$ increases from 0.8 to 1.6. However, at 150 °C, the decrease in foaming time is from 3 to 1.5 h. The corresponding decrease in foam setting time is from 98 to 32.75 h at 120 °C and 21 to 9 h at 150 °C.

The foam rise, a measure of foam volume, is the ratio of the final foam height to the initial dispersion height. Fig. 2 shows the effect of temperature and $W_{A/S}$ on the foam rise of alumina powder dispersions in molten sucrose. At all studied $W_{A/S}$, the foam rise increases with an increase in foaming temperature, reaches a maximum at a certain temperature (hereafter called as critical foaming temperature) and then decreases. The decrease of foam rise beyond the critical foaming temperature is due to the foam collapse. The critical foaming temperature decreases with an increase in the $W_{A/S}$. That is, the critical foaming temperature decreases from 170 to 140 °C when the $W_{A/S}$ increases from 0.8 to 1.6. On the other hand, below the critical foaming temperature, the foam rise of dispersion shows only a minor variation with $W_{A/S}$.

The foaming involves nucleation and growth of bubbles in the fluid medium. The nucleation of bubbles depends on the rate of formation of water molecules, which depends on the rate of —OH condensation. The growth of bubbles involves diffusion of water vapour to the nucleated bubbles. That is, the bubble growth depends on the rate of formation as well as the rate of diffusion of the water vapour through the medium. In addition, the bubble growth in a viscous medium is opposed by the viscous forces. A low viscosity is desirable to offer lower resistance to bubble growth and faster diffusion of water vapour. On the other hand, the viscosity plays a major role in the stabilization of the formed bubbles. A higher viscosity is desirable for the bubble stabilization. Fig. 3 shows the effect of temperature and $W_{A/S}$ on the viscosity of alumina powder dispersions in molten sucrose measured at a shear rate of 10 s^{-1}. The relatively high viscosity of the dispersions is due to strong intermolecular hydrogen bonding between the sucrose molecules. The decrease in viscosity with an increase in temperature is due to the weakening of the intermolecular hydrogen bonding as well as an increase in molecular mobility. At a particular temperature, the viscosity of the dispersions increases with an increase in $W_{A/S}$ due to the increased interparticle Van der Waals interactions [31]. This effect is more dominant at lower temperatures. The viscosity increase is slow up to a $W_{A/S}$ of 1.4 and thereafter rapid. For example, the viscosity at 120 °C increases slowly from 25.5 to 44.4 Pa s when the $W_{A/S}$ increases from 0.8 to 1.4. Further increase in the $W_{A/S}$ to 1.6 results in a rapid increase in the viscosity of the dispersion to 117 Pa s. At $W_{A/S}$ beyond 1.6, dispersion shows enormously high viscosities. For example, the dispersion at a $W_{A/S}$ of 1.8 shows a viscosity of 1140 Pa s at 120 °C. No foaming is observed in the dispersion at a $W_{A/S}$ of 1.8 at temperatures in the range of 120–180 °C due to the high viscosity. The decrease in foaming time and foam setting time with an increase in temperature is due to the increase in the rate of —OH condensation. The increase in foam rise with an increase in foaming temperature is due to the increase in the rate of —OH condensation as well as a decrease in viscosity of the dispersions. On the other hand, the decrease in foaming time and foam setting time and increase in foam rise with an increase in $W_{A/S}$ at a given foaming temperature is due to the catalytic effect of alumina towards —OH condensation as well as stabilization of bubbles by both viscosity increase and adsorption of the alumina particles on the bubble surface [29].

The foam collapse observed beyond the critical foaming temperature is due to the rupture of bubbles when the pressure inside the bubbles exceeds the strength of cell walls. There are two possible reasons for the decrease in critical foaming temperature with an increase in $W_{A/S}$. As the alumina powder catalyzes the —OH condensation, the rate of —OH condensation increases with an increase in $W_{A/S}$, which results in an increase of pressure inside the bubbles at lower temperature leading to their rupture. On the other hand, as the $W_{A/S}$ increases, the population of alumina particle agglomerates increases. This alumina particle agglomerates limit the strength of cell walls leading to their rupture at lower pressure inside the bubbles, at lower temperatures.

The sucrose polymer–alumina powder composite foam bodies undergo relatively large shrinkage during sintering. Fig. 4 shows the effect of $W_{A/S}$ and foaming temperature on the total volume shrinkage (shrinkage during pyrolysis and sintering) during sintering of sucrose polymer–alumina powder composite bodies. The volume shrinkage during sintering increases with a decrease in the $W_{A/S}$. On the other hand, the foam bodies prepared at a particular $W_{A/S}$ show only a marginal decrease in volume shrinkage with an increase in foaming temperature. The composite foam bodies prepared at various foaming temperatures at a $W_{A/S}$ have more or less same composition but different foam volume due to a difference in the cell size. The sintering shrinkage depends largely on the alumina powder loading in the composite foam and not on the foam volume (cell size).

The alumina foams show interconnected cellular structure irrespective of the $W_{A/S}$ and foaming temperature. At all studied $W_{A/S}$ thermo-foaming produces near-spherical cells up to the critical

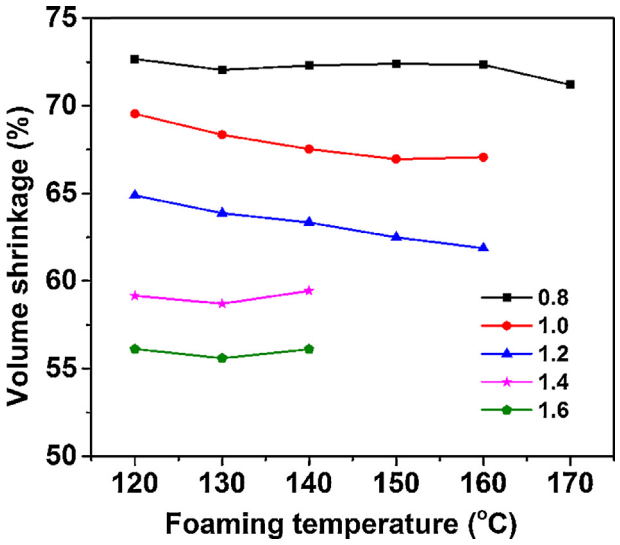

Fig. 4. Effect of $W_{A/S}$ and foaming temperature on sintering shrinkage of foam bodies.

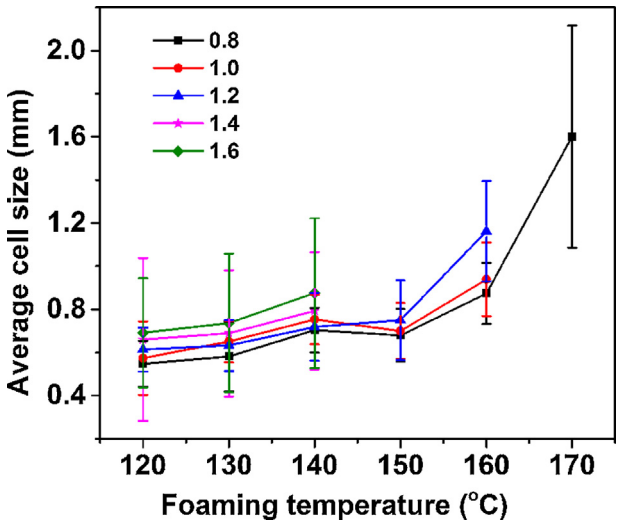

Fig. 6. Effect of foaming temperature and $W_{A/S}$ on the average cell size of alumina foams.

foaming temperature. On the other hand, the partially collapsed foam obtained beyond the critical foaming temperature contains oval-shaped cells. The SEM photomicrograph of the alumina foams prepared at various foaming temperatures at a $W_{A/S}$ of 1 is shown in Fig. 5. The spherical cells up to the critical foaming temperature (160 °C at $W_{A/S}$ of 1) and a change in shape of the cells from spherical to oval beyond the critical foaming temperature are clearly evidenced from the SEM photomicrograph. The increase in cell size due to bubble growth with an increase of foaming temperature is also evidenced from the microstructure. Similar cell structure and a similar change in cell structure beyond the critical foaming temperature are observed at all studied $W_{A/S}$.

Fig. 6 shows the effect of foaming temperature on the average cell size of the alumina foams prepared at various $W_{A/S}$. At a particular foaming temperature, the cell size of alumina foams shows only a marginal increase with an increase in $W_{A/S}$. For example, the average cell size of alumina foam prepared at a foaming temperature of

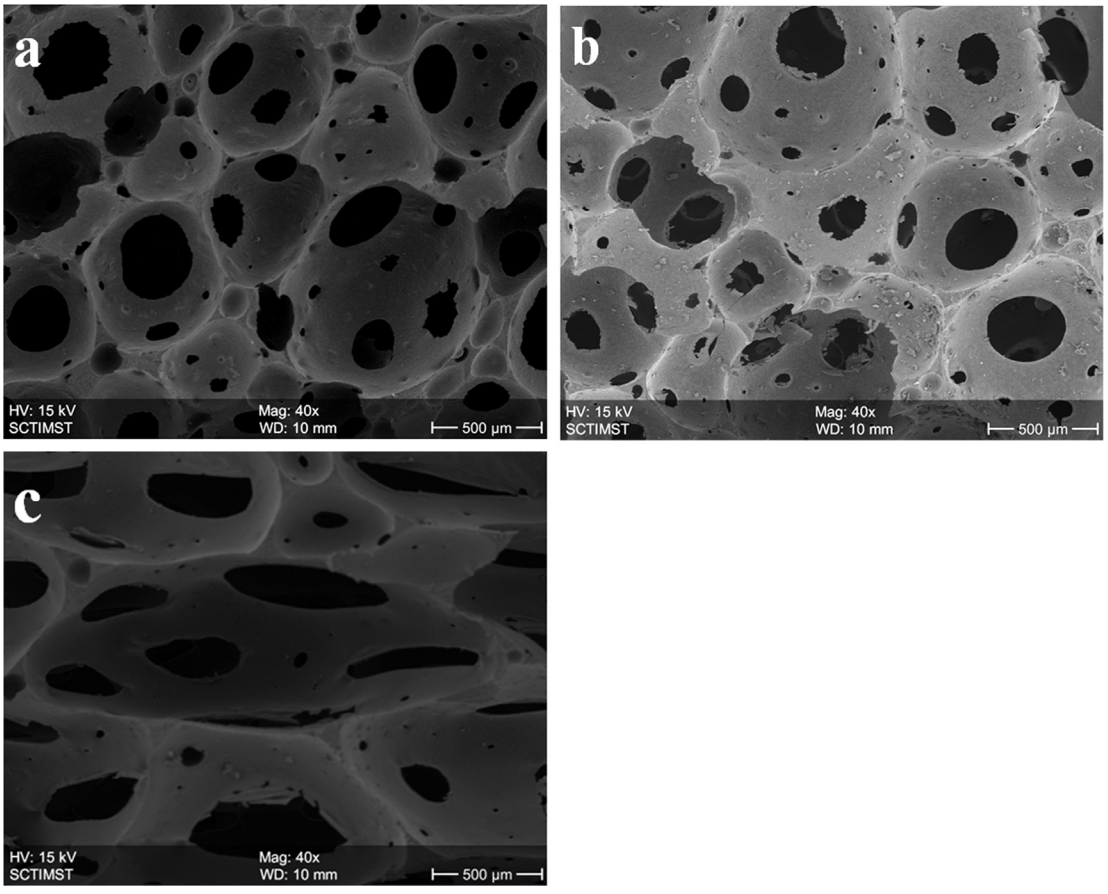

Fig. 5. The SEM photomicrograph of alumina foams prepared at the foaming temperatures of (a) 120 °C, (b) 160 °C and (c) 170 °C at a $W_{A/S}$ of 1.

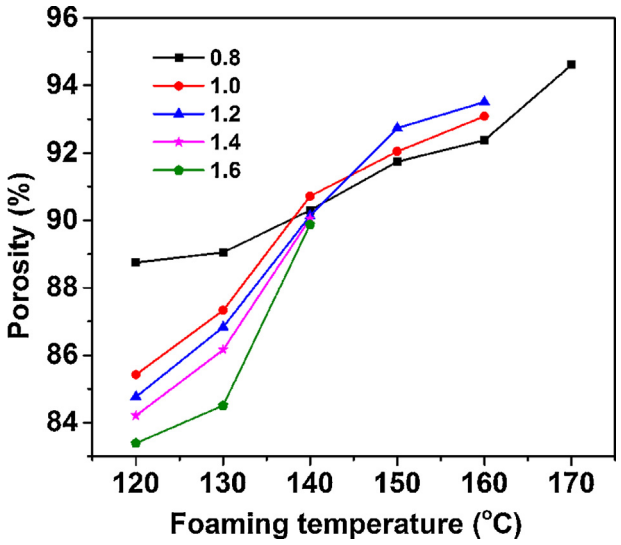

Fig. 7. Effect of foaming temperature and $W_{A/S}$ on porosity of alumina foams.

120 °C increases from 0.55 to 0.7 mm when the $W_{A/S}$ increases from 0.8 to 1.6. On the other hand, the cell size of alumina foams prepared at various $W_{A/S}$ shows a considerable increase with an increase in foaming temperature. The increase in cell size is gradual up to a foaming temperature of 150 °C and thereafter rapid. The increase in cell size with an increase in foaming temperature is because of an enhanced bubble growth due to an increase in the rate of —OH condensation and a decrease in the viscosity of the dispersion. The study suggests that the average cell size of alumina foams could be controlled in a wide range of 0.55–1.6 mm by controlling the $W_{A/S}$ and foaming temperature.

The porosity of the alumina foam prepared at a particular $W_{A/S}$ increases with an increase in foaming temperature up to the critical foaming temperature. The increase in porosity is due to the increase in cell size with an increase in foaming temperature. Beyond the critical foaming temperature decrease in porosity due to the densification by partial foam collapse is observed. On the other hand, at foaming temperatures in the range of 120–140 °C, the porosity shows a marginal decrease with an increase in $W_{A/S}$ even though the cell size shows a marginal increase. The observed decrease in porosity with an increase in $W_{A/S}$ is attributed to an increase in the strut thickness [29]. However, a reverse trend in porosity with an increase in $W_{A/S}$ is observed at foaming temperatures above 140 °C. The alumina foams with porosity in the wide range of 83.4–94.6 vol.% could be prepared from alumina powder dispersions in molten sucrose by thermo-foaming at temperatures in the range of 120–170 °C. Fig. 7 shows the effect of foaming temperature and $W_{A/S}$ on the porosity of alumina foams.

The compressive strength of macroporous brittle solids depends on the porosity, pore size, pore interconnectivity and thickness of the cell wall and strut [28,30–32]. The compressive strength decreases with an increase in porosity, increase in cell size and increase in cell interconnectivity and decrease in strut thickness. The effect of foaming temperature on the compressive strength and Young's modulus of the alumina foams prepared at various $W_{A/S}$ is shown in Fig. 8. At all studied $W_{A/S}$ the compressive strength decreases with an increase in foaming temperature as the porosity and cell size of the foams increase. For example, the compressive strength of alumina foam prepared at a $W_{A/S}$ of 1 decreases from 8.53 to 1.13 MPa when the foaming temperature increases from 120 to 160 °C due to an increase in porosity from 85.4 to 93 vol.% and an increase in cell size from 0.57 to 0.94 mm. Similarly, at a given foaming temperature, the compressive strength of alumina

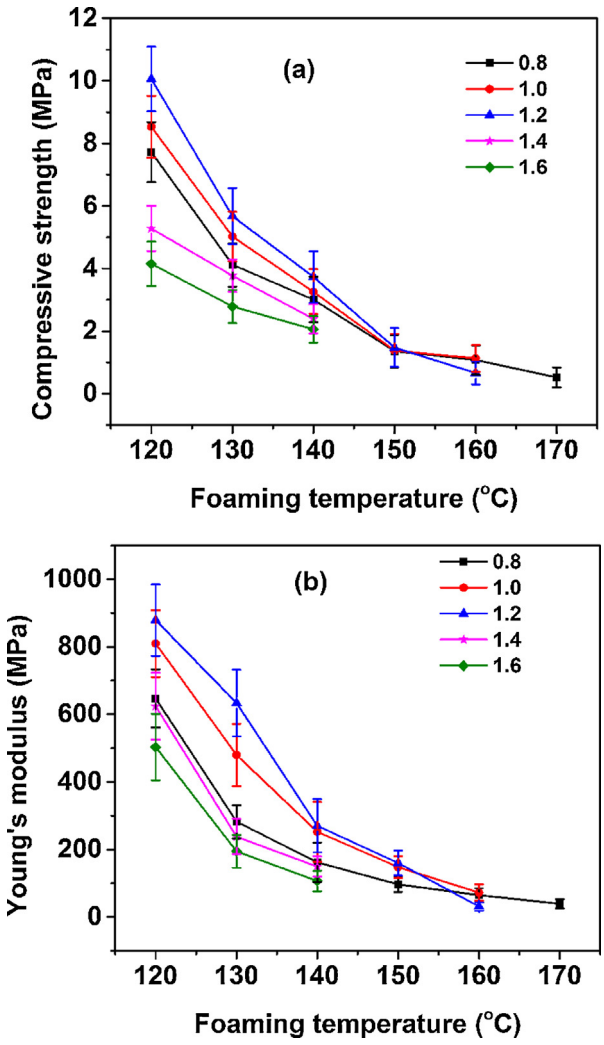

Fig. 8. Effect of foaming temperature and $W_{A/S}$ on (a) compressive strength and (b) Young's modulus of the alumina foams.

foams prepared at the $W_{A/S}$ in the range of 0.8–1.2 shows a marginal increase with an increase in the $W_{A/S}$. This is attributed to the marginal decrease in porosity and increase in strut thickness with an increase in $W_{A/S}$ [29]. The Young's modulus of the alumina foams shows a similar trend with the foaming temperature and $W_{A/S}$. For example, the Young's modulus at $W_{A/S}$ of 1 decreases from 809.4 to 72.5 MPa when the foaming temperature increases from 120 to 160 °C. On the other hand, the alumina foams prepared at the $W_{A/S}$ of 1.4 and 1.6 show lower compressive strength and Young's modulus than that of the foam prepared at a $W_{A/S}$ of 0.8.

The lower compressive strength and Young's modulus of alumina foams at the $W_{A/S}$ of 1.4 and 1.6 in spite of their lower porosity demand detailed investigation of their microstructure. The microstructure of the alumina foams prepared at the $W_{A/S}$ of 1.4 and 1.6 contains a large number of pinholes on the cell walls. In addition, larger numbers of micro-bubbles are observed in the struts. Also, the high magnification SEM images shows micropores in inter- and intra-granular regions. Fig. 9 shows typical SEM microstructures showing pinholes on the cell walls, micro bubbles in the struts and micropores in the inter- and intra-granular region in the foam prepared at a $W_{A/S}$ of 1.4. It appears that alumina powder disperses well in molten sucrose up to a $W_{A/S}$ of 1.2 (volume % of alumina 32.4). The agglomeration of alumina particles in the molten sucrose medium starts at a $W_{A/S}$ beyond 1.2. This is clearly evidenced in the increase in viscosity with alumina powder to sucrose weight ratio

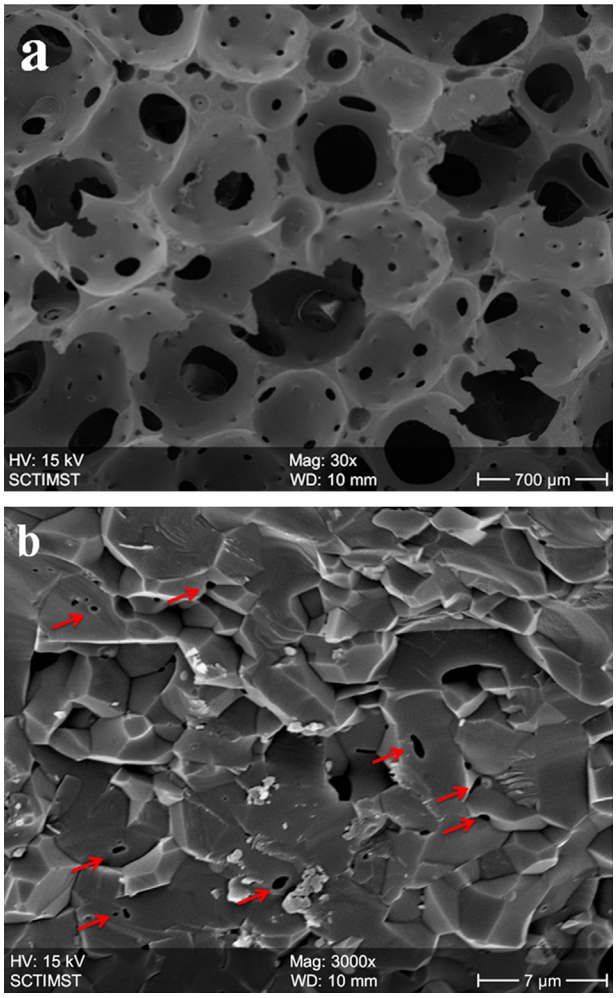

Fig. 9. SEM photomicrograph of alumina foam at a $W_{A/S}$ of 1.4 showing (a) pinholes on the cell walls and struts and (b) inter- and intra-granular porosity.

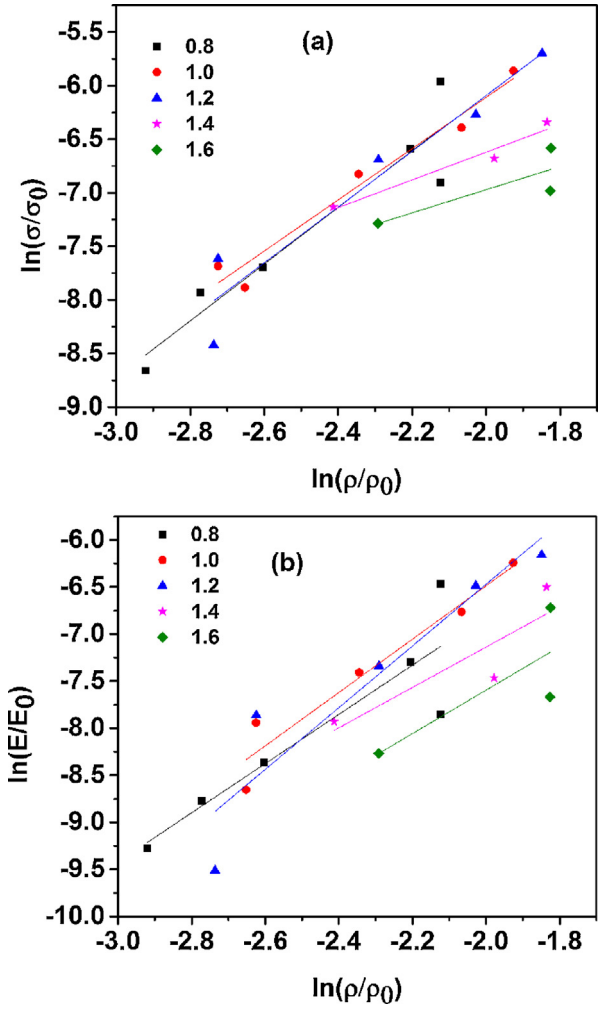

Fig. 10. Logarithmic plots of (a) σ/σ_0 against ρ/ρ_0 and (b) E/E_0 against ρ/ρ_0.

of the dispersions (Fig. 3). The sintering of these particle agglomerates creates pinholes on the cell walls and struts and micropores in inter- and intra-granular region. It appears that the bubbles nucleated in the thick struts during the later stages of the foaming of alumina powder dispersions or initial stages of foam setting are stabilized due to the high viscosity at higher $W_{A/S}$. It is well known that the pores present in the struts limits the strength of brittle foam materials [33]. The lower strength and Young's modulus of foams prepared at the $W_{A/S}$ 1.4 and 1.6 are due to the pinholes present on the cell walls, higher population of the micro bubbles in the struts and micro pores present in the inter- and intra-granular regions.

The Young's modulus of brittle open cellular solids is best modelled using Eq. (1) proposed by Gibson and Ashby [32]:

$$\frac{E}{E_0} = C\left(\frac{\rho}{\rho_0}\right)^n \quad (1)$$

where E_0 and E are the Young's moduli of the fully dense solid and open cellular solid, respectively. The C and n are constants depending on the pore geometry and microstructure. A similar equation [34] can be used for the modelling of the compressive strength. The plots of $\ln(\sigma/\sigma_0)$ versus $\ln(\rho/\rho_0)$ and $\ln(E/E_0)$ versus $\ln(\rho/\rho_0)$ of alumina foams prepared at various foaming temperatures and $W_{A/S}$ are shown in Fig. 10. The model plots are generated by considering the strength (σ_0) and Young's modulus (E_0) of fully dense alumina ceramic as 3 GPa and 416 GPa, respectively [35]. The values of model constants C and n as well as the correlation coefficient R^2 are given in Table 1. The correlation coefficient close to one indicates a high degree of matching between the experimental results with the model graph. The compressive strength and Young's modulus data show moderate value of correlation coefficients at the $W_{A/S}$ in the range of 0.8–1.4. On the other hand, very low values of correlation coefficients are obtained at a $W_{A/S}$ of 1.6. The values of C

Table 1
Values of model constants C, n and correlation coefficient R^2.

$W_{A/S}$	Compressive strength			Young's modulus		
	n	C	R^2	n	C	R^2
0.8	2.6439	0.45282	0.80715	2.61536	0.2066	0.76755
1.0	2.39182	0.26553	0.95627	2.54939	0.23939	0.92145
1.2	2.60297	0.41217	0.90459	3.27825	0.30570	0.83479
1.4	1.29276	0.13061	0.922	2.14521	0.0579	0.56829
1.6	1.08198	0.06039	0.3668	2.30915	0.50986	0.26453

and n for the relation between E/E_0 and ρ/ρ_0 are expected to be ~1 and ~2, respectively, for brittle open cellular foams with a cubic array of cells [32,36,37]. The values for 'C' and 'n' largely deviate from the values predicted by Gibson and Ashby, especially at higher $W_{A/S}$ of 1.4 and 1.6. The Gibson and Ashby model is based on completely interconnected foam with an array of cubic cells of uniform size. The large deviation in the values of 'C' and 'n' and low value of correlation coefficient at the $W_{A/S}$ of 1.4 and 1.6 is attributed to the pinholes on the cell walls and microbubbles present in the struts as well as deviation in the cell shape.

4. Summary

The thermo-foaming of alumina powder dispersions in molten sucrose at $W_{A/S}$ in the range of 0.8–1.8 is carried out at temperatures in the range of 120–180 °C for the preparation of alumina foams. The foaming and foam setting time of alumina powder dispersions decrease with an increase in foaming temperature and an increase in $W_{A/S}$. The foam volume increases considerably with an increase in foaming temperature, reaches a maximum at a critical foaming temperature and then decreases due to foam collapse. The critical foaming temperature decreases with an increase in the $W_{A/S}$. A decrease in foaming and foam setting time and an increase in foam volume with an increase in foaming temperature are due to an increase in the rate of —OH condensation as well as a decrease in viscosity of the dispersion. The sintering shrinkage decreases largely with an increase in $W_{A/S}$and marginally with an increase in foaming temperature. The porosity (83.4–94.6 vol.%) and average cell size (0.55–1.6 mm) of alumina foams increase considerably with an increase in foaming temperature at a particular $W_{A/S}$ and decrease marginally with an increase in $W_{A/S}$ at a particular foaming temperature. The compressive strength and the Young's modulus of the alumina foams modelled according to the equations proposed by Gibson and Ashby showed moderate to low correlation coefficient and large deviation in model constants such as C and n, especially at higher $W_{A/S}$.

Acknowledgements

The authors are thankful to Dr. K.S. Dasgupta, Director, Dr. Kuruvilla Joseph, Dean Student Activities and Dr. Nirmala Rachel James, Head of the Department of Chemistry of IIST for their encouragements.

References

[1] A.R. Studart, U.T. Gonzenbach, E. Tervoortand and L.J. Gauckler, J. Am. Ceram. Soc., 89, 1771–1789 (2006).
[2] J. Sagggio-Woyansky and C.E. Scott, Am. Ceram. Soc. Bull., 71, 1674–1682 (1992).
[3] M. Takahashi, R.L. Menchavez, M. Fuji and H. Takegami, J. Eur. Ceram. Soc., 29, 823–828 (2009).
[4] J. Binner, H. Chang and R. Higginson, J. Eur. Ceram. Soc., 29, 837–842 (2009).
[5] H. Haugen, J. Will, A. Köhler, U. Hopfner, J. Aigner and E. Wintermantel, J. Eur. Ceram. Soc., 24, 661–668 (2004).
[6] R. Faure, F. Rossignol, T. Chartier, C. Bonhomme, A. Maître, G. Etchegoyen, P.D. Gallo and D. Gary, J. Eur. Ceram. Soc., 31, 303–312 (2011).
[7] K. Schwartzwalder, A.V. Somers, US Patent 3 090 094 (1963).
[8] J.W. Brockmeyer, US Patent 4 610 832 (1986).
[9] X.W. Zhu, D.L. Jiang and S.H. Tan, J. Inorg. Mater., 16, 1144–1150 (2001).
[10] P. Sepulveda, Am. Ceram. Soc. Bull., 76, 61–65 (1997).
[11] P. Sepulveda and J.G.P. Binner, J. Eur. Ceram. Soc., 19, 2059–2066 (1999).
[12] J.G.P. Binner, Br. Ceram. Trans., 96, 247–249 (1997).
[13] X. Mao, S. Shimai and S. Wang, J. Eur. Ceram. Soc., 28, 217–222 (2008).
[14] F.S. Ortega, P. Sepulveda and V.C. Pandolfell, J. Eur. Ceram. Soc., 22, 1395–1401 (2002).
[15] F.S. Ortega, F.A.O. Valenzuel, C.H. Scuracchio and V.C. Pandolfelli, J. Eur. Ceram. Soc., 23, 75–80 (2003).
[16] I. Garrn, C. Reetz, N. Brandes, L.W. Krohb and H. Schubert, J. Eur. Ceram. Soc., 24, 579–587 (2004).
[17] B.P. Binks and T.S. Horozov, Angew. Chem. Int. Ed., 44, 3722–3725 (2005).
[18] U.T. Gonzenbach, A.R. Studart, E. Tervoort and L.J. Gauckler, Angew. Chem. Int. Ed., 45, 3526–3530 (2006).
[19] U.T. Gonzenbach, A.R. Studart, D. Steinlin, E. Tervoort and L.J. Gauckler, J. Am. Ceram. Soc., 90, 3407–3414 (2007).
[20] A. Imhof and D.J. Pine, Nature, 389, 948–951 (1997).
[21] A. Imhof and D.J. Pine, Adv. Mater., 10, 697–700 (1998).
[22] V.N. Manoharan, A. Imhof, J.D. Thorne and D.J. Pine, Adv. Mater., 13, 447–450 (2001).
[23] S. Barg, C. Soltmann, M. Andrade, D. Koch and G. Grathwohl, J. Am. Ceram. Soc., 91, 2823–2829 (2008).
[24] S. Barg, E.G. de Moraes, D. Koch and G. Grathwohl, J. Eur. Ceram. Soc., 29, 2439–2446 (2009).
[25] E.M.M. Ewais, S. Barg, G. Grathwohl, A.A. Garamoon and N.N. Morgan, Int. J. Appl. Ceram. Technol., 8, 85–93 (2011).
[26] M.A. Alves-Rosa, L. Martins, S.H. Pulcinelli and C.V. Santilli, Soft Matter, 9, 550–558 (2013).
[27] S. Vijayan, R. Narasimman and K. Prabhakaran, J. Eur. Ceram. Soc., 34, 4347–4354 (2014).
[28] S. Vijayan, R. Narasimman and K. Prabhakaran, J. Asian Ceram. Soc., 3, 279–286 (2015).
[29] S. Vijayan, R. Narasimman, C. Prudvi and K. Prabhakaran, J. Eur. Ceram. Soc., 34, 425–433 (2014).
[30] S. Vijayan, R. Narasimman and K. Prabhakaran, J. Mater. Res., 31, 302–309 (2016).
[31] G.D. Parfitt, Fundamental aspects of dispersion in Dispersion of Powders in Liquids, Ed. by G.D. Parfitt, Applied Sciences, New Jersey (1981) pp. 1–47.
[32] L.J. Gibson and M.F. Ashby, Cellular Solids: Structure and Properties, 2nd ed., Cambridge University Press: Cambridge Solid State Press, Cambridge (1997), pp. 183–200.
[33] I. Jun, Y. Koh, J. Song, S. Lee and H. Kim, Mater. Lett., 60, 2507–2510 (2006).
[34] J. Verma, R. Mitra and M. Vijayakumar, J. Eur. Ceram. Soc., 33, 943–951 (2013).
[35] R.G. Munro, J. Am. Ceram. Soc., 80, 1919–1928 (1997).
[36] F.A. Costa Oliveira, S. Dias, M. Fátima Vaz and J. Cruz Fernandes, J. Eur. Ceram. Soc., 26, 179–186 (2006).
[37] J.S. Magdeski, J. Univ. Chem. Technol. Metall., 45, 143–148 (2010).